Article

Not peer-reviewed version

Effects of Simulated Acid Rain on Photosynthesis in *Pinus massoniana* and *Cunninghamia lanceolata* in Terms of Prompt Fluorescence, Delayed Fluorescence, and Modulated Reflection at 820 nm

Pengzhou Shu , Xiaofei Gong , Yanlei Du , Yini Han , Songheng Jin , Zhongxu Wang , Penghong Qian , Xueqin Li *

Posted Date: 10 January 2024

doi: 10.20944/preprints202401.0791.v1

Keywords: simulated acid rain; chlorophyll a fluorescence induction kinetics; 820-nm transmission kinetics; JIP-test; delayed fluorescence; coniferous trees

Article

Effects of Simulated Acid Rain on Photosynthesis in *Pinus massoniana* and *Cunninghamia lanceolata* in Terms of Prompt Fluorescence, Delayed Fluorescence, and Modulated Reflection at 820 nm

Pengzhou Shu [1], Xiaofei Gong [2], Yanlei Du [3], Yini Han [1], Songheng Jin [1], Zhongxu Wang [1], Penghong Qian [1] and Xueqin Li [1,*]

[1] Jiyang College, Zhejiang A&F University, Zhuji, China
[2] Ecological Forestry Development Center of Suichang County, Suichang, China
[3] Environmental Protection Monitoring Station of Changxing County, Changxing, Zhejiang Province, China
* Correspondence: Xueqin Li, lxqin@zafu.edu.cn

Abstract: The effects of simulated acid rain (SAR) on the photosynthetic performance of subtropical coniferous species have not been thoroughly investigated. In this study, we treated two coniferous species, *Pinus massoniana* (PM) and *Cunninghamia lanceolata* (CL), with SAR and then analyzed photosynthetic activities via the simultaneous measurement of prompt fluorescence(PF), delayed fluorescence(DF), and modulated reflection at 820 nm(MR_{820}). Following the low-pH SAR treatment, the I–P phase of the OJIP curves of PM and CL decreased significantly and then the K-band and L-band were detectable. The delayed fluorescence for both PM and CL decreased as the pH of the SAR solution decreased, with a more significant decrease in the I_1 peak than in the I_2 peak. According to the MR_{820} curve, the exposure to SAR stress inhibited the rapid decrease and slow increase in the MR_{820} transients of PM and CL. The gradients of the decreasing and increasing phases were lower for CL than for PM at pH 2.5. In addition, SAR decreased the light energy captured per unit area (ABS/CS_m) and the quantum yield of electron transfer per unit area (ET_O/CS_m), but it increased the accumulation of QA^-, thereby decreasing primary photochemical efficiency (TR_O/CS_m, φP_O). These changes in photosystem II (PSII) resulted in a decrease in the maximum quantum yield of PSII (F_v/F_m) and the performance index (PI_{ABS}). Moreover, PSII was protected from thylakoid membrane photodamages through the increase in heat dissipation per unit area (DI_O/CS_m) in response to SAR. The increase in δR_O as the pH of the SAR solution decreased was observed for PM, but not for CL. Considered together, the study findings suggest that SAR treatments can decrease chlorophyll contents and damage the OEC in PM and CL, which obstructs the transfer of electrons on the donor and acceptor sides of PSII. However, PM is better able to withstand SAR stress than CL, likely because of the activation of a protective mechanism (reflected by the change in δR_O). Therefore, in coniferous forest areas severely affected by acid rain, CL may need to be protected more than PM.

Keywords: simulated acid rain; chlorophyll a fluorescence induction kinetics; 820-nm transmission kinetics; JIP-test; delayed fluorescence; coniferous trees

1. Introduction

Acid rain has become one of the most serious environmental problems worldwide because of decades of industrial development as well as increases in energy demands and emissions of certain gases, including sulfur dioxide (SO_2) and nitrogen oxides (NO_X) (Shi et al., 2021). In terms of the total area affected by acid rain, China ranks third behind Europe and North America (Tomlinson et al., 2003). The acid rain-affected regions in China account for 3.8% of the total land area, with Zhejiang province among the regions severely affected by acid rain (average acid rain rate of 47.9%) (Ling et al., 2010). According to Li et al. (2021), because of improvements in the energy supply structure (e.g., use of renewable energy sources) and significant increases in NO_X emissions from vehicle exhausts, the main acids associated with acid rain in the subtropical region have recently changed from mainly sulfuric acid to a mixture of sulfuric acid and nitric acid. Despite the active efforts of government

 doi:10.20944/preprints202401.0791.v1

departments to control acid rain and mitigate its adverse effects, there are still major environmental problems due to acid rain in the subtropical region.

Simulated acid rain (SAR) initially affects plants by damaging the leaf wax, which leads to the rupture of the epidermis (Du et al., 2017). Additionally, the outer stomatal wall on the abaxial side of leaves also ruptures in response to SAR. The morphology of some epidermal cells is consistent with the effects of lysis. Plants accumulate phenolic compounds in necrotic areas. A subsequent exposure to low-pH stress can damage the leaf mesophyll, ultimately leading to the complete collapse of mesophyll cells (Sant'Anna-Santos et al., 2006). Moreover, SAR can also alter the physical and chemical properties of soil, thereby affecting the absorption of water and nutrients by plant roots, inhibiting plant growth and development, exacerbating plant diseases and pest infestations, accelerating leaf yellowing and shedding, and leading to the severe degradation of terrestrial ecosystems (Wu et al., 2002; Liang et al., 2008). Many studies on SAR that mainly focused on its effects on soil microorganisms in the plant rhizosphere revealed that SAR primarily affects soil respiration and soil physicochemical properties (Lv et al., 2013; Berger et al., 2015; Li et al., 2021;Zheng et al., 2022;Zhang et al., 2023). For evergreen trees in the subtropical region, only low pH acidic conditions have a significant effect, while high pH would not (Shi et al., 2021). Studies have been conducted on the effects of SAR on plant leaves (Francisco et al., 2005; Du et al., 2017) and nutrient elements (Diatta et al., 2020). Recent studies have explored how the frequency of SAR influences soil microorganisms and plants (Liu et al., 2020). There has been considerable research on the effects of SAR on the morphological features and photosynthetic activities of plants. More specifically, the related research on economically important coniferous species, such as *Pinus massoniana* (PM) and *Cunninghamia lanceolata* (CL), treated with SAR has mainly focused on biological characteristics, including growth (Zhang et al., 2023), physiological functions (Ren et al., 2013; Fan et al., 2005), wood or fruit quality (Liu et al., 1996), and ecological functions (Wang et al., 2012; Liu et al., 2010).

In terms of plant physiology, subtropical evergreen broad-leaved trees are more tolerant to acidic conditions than coniferous trees (Malla et al.,2023). This is in accordance with the results of an earlier study involving an examination of spectral reflectance, which indicated coniferous tree species are more sensitive to SAR than broad-leaved tree species (Shi et al.,2021). There are few reports describing the changes in the growth characteristics and photosynthetic performance of PM and CL in response to SAR. In addition to being the most representative coniferous tree species in the subtropical region, PM and CL are the most widely cultivated timber species in China (Jiang et al., 2017; Yin et al., 2009; Shan et al., 1988; Sun et al., 2020).

The development of the Multi-Function Plant Efficiency Analyzer (M-PEA) for the simultaneous measurement of prompt chlorophyll fluorescence (PF), delayed chlorophyll fluorescence (DF), and modulated reflection (MR) enabled the examination of the changes in forward and reverse electron transport and/or the redox state of photosystem I (PSI) in many plant species (Strasser et al,2010; Oukarroum et al, 2013). The correlations among the aforementioned signals can provide mutually corroborating and complementary insights into the photosynthetic electron transport chain, including the forward and reverse electron flow and the cyclic electron flow around PSI. A previous study verified the utility of PF, DF, and the MR at 820 nm (MR_{820}) curve for analyzing the degree of plant stress (Zhou et al.,2018). The PF increases in three phases (O–J, J–I, and I–P), which represent three distinct reduction reactions in the electron transport chain. During photosynthesis, PF is detectable after the dark-to-light transition, whereas DF can be detected during the light-to-dark transition (Strasser et al., 2010). In addition, DF is mainly emitted by photosystem II (PSII) rather than PS I (Jursinic et al., 1986). Based on this energy cascade, PF emitted by chlorophyll a reflects the photosynthetic vitality, especially for PSII, and can be measured under saturated actinic light at a wavelength of 627 ± 10 nm(Zushi et al., 2017). The transient MR signals at 820 nm suggest the transport of electrons beyond the plastoquinone (PQ) pool in PSI can be measured under modulated light at a wavelength of 820 ± 25 nm. The DF denoting the charge recombination and re-population of excited PSII antenna chlorophyll can be measured under far-red light at a wavelength of 735 ± 15 nm (Goltsev. et al, 2009; Strasser et al, 2010).

Preprints (www.preprints.org) | NOT PEER-REVIEWED | Posted: 10 January 2024 doi:10.20944/preprints202401.0791.v1

To date, PF, DF, and the MR820 curve have been widely used during analyses of the effects of heat stress (Chen et al.,2015), salt stress (Kan et al.,2017), drought stress (Liu et al.,2018), and heavy metal stress (Poschenrieder et al.,2008). However, there have been relatively few studies that combined PF, DF, the MR_{820} curve, and JIP-test parameters to investigate the mechanism underlying the response of coniferous tree species to SAR. The objectives of this study were to use the above-mentioned methods to elucidate the mechanism mediating the response of subtropical coniferous species to SAR and to reveal the diversity in the responses of subtropical coniferous species to SAR, thereby providing the theoretical basis for developing effective methods for protecting subtropical coniferous species from acid rain.

2. Results

The SAR treatment inhibited PM and CL growth (Figure 1). Decreases in the pH of the SAR solution resulted in decreases in the tree height and stem diameter of both species. At pH 4.0, the tree height of CL decreased more than that of PM. Additionally, the stem diameter of CL decreased more significantly than that of PM at pH 2.5.

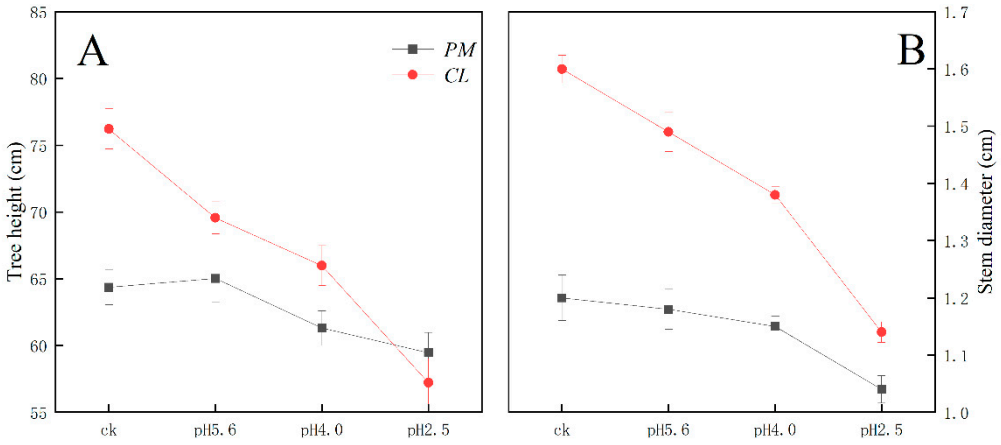

Figure 1. Effects of SAR stress on PM and CL tree height and stem diameter.

The gas exchange parameters of PM and CL following the SAR treatments are presented in Figure 2. The application of the SAR solutions significantly decreased Pn and Gs for both PM and CL, whereas Ci increased as the SAR stress increased. After the SAR treatments, Pn and Gs were higher for PM than for CL, whereas the opposite trend was observed for Ci. Compared with the effects of the control treatment, the SAR pH 2.5 treatment of PM and CL resulted in decreases in Pn (by 82.04% and 84.14%, respectively) and Gs (by 81.10% and 84.88%, respectively), but increases in Ci (by 36.02% and 40.37%, respectively).

Preprints (www.preprints.org) | NOT PEER-REVIEWED | Posted: 10 January 2024 doi:10.20944/preprints202401.0791.v1

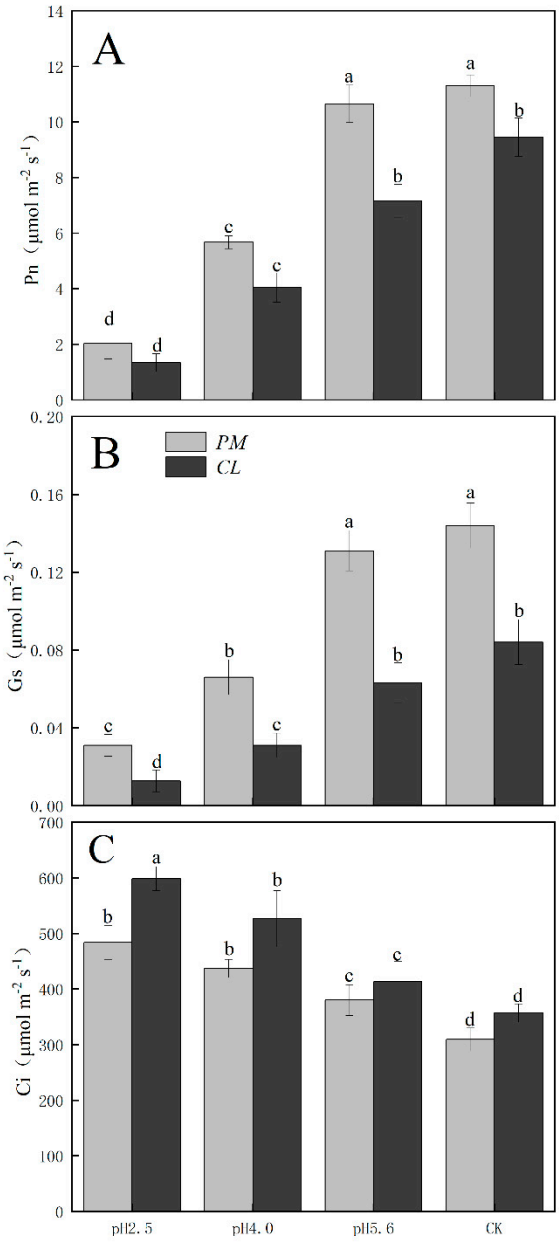

Figure 2. Effects of SAR on gas exchange in PM and CL. (A) Net photosynthetic rate (Pn). (B) Stomatal conductance (Gs). (C) Intercellular CO_2 concentration (Ci).

The photosynthetic pigment contents in PM and CL decreased as the pH of the SAR solution decreased. Moreover, there was a negative correlation between the photosynthetic pigment content and the SAR stress level (Figure 3). The changes in the chlorophyll A, chlorophyll B, and total chlorophyll contents were similar between PM and CL. At pH 2.5, the chlorophyll A contents of PM and CL decreased by 49.00% and 89.04%, respectively. The chlorophyll B contents of PM and CL decreased by 54.74% and 82.20%, respectively. The total chlorophyll contents of PM and CL decreased by 50.14% and 87.75%, respectively. There was no significant change in the carotenoid content of PM as the pH of the SAR solution decreased, whereas the carotenoid content of CL decreased significantly more after the SAR pH 2.5 treatment (by 63.96%) than after the SAR pH 4.0 or 5.6 treatments.

Preprints (www.preprints.org) | NOT PEER-REVIEWED | Posted: 10 January 2024 doi:10.20944/preprints202401.0791.v1

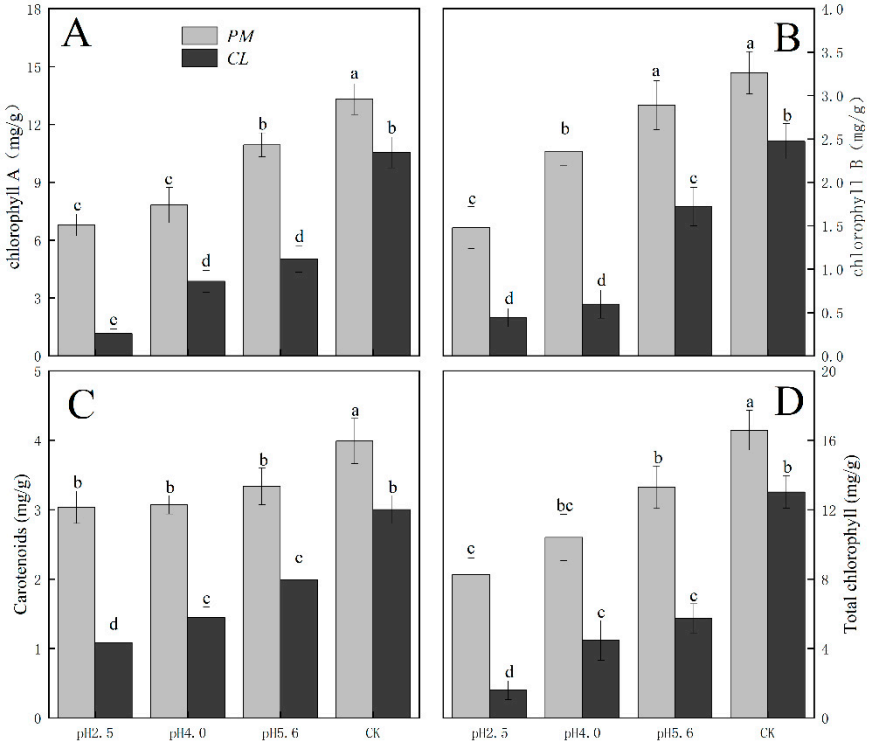

Figure 3. Photosynthetic pigment contents in PM and CL under SAR stress conditions. (A) Chlorophyll A. (B) Chlorophyll B. (C) Carotenoids. (D) Total chlorophyll.

Distinct OJIP curves were generated for both PM and CL treated with different SAR solutions. As the pH of the SAR solution decreased, the I–P phase of the OJIP curve decreased significantly (Figure 4). However, there was a difference between the two species. More specifically, the overall curve of PM decreased as the pH decreased, but the curve of CL revealed an increase in F_O as the pH decreased. Furthermore, in response to the decrease in pH, the OJIP curve gradually transformed into an OKJIP curve with an obvious K-band. In addition, following the SAR pH 2.5 and 4.0 treatments, the P point was eventually undetectable in the CL curve, whereas it was still detectable in the PM curve.

Preprints (www.preprints.org) | NOT PEER-REVIEWED | Posted: 10 January 2024 doi:10.20944/preprints202401.0791.v1

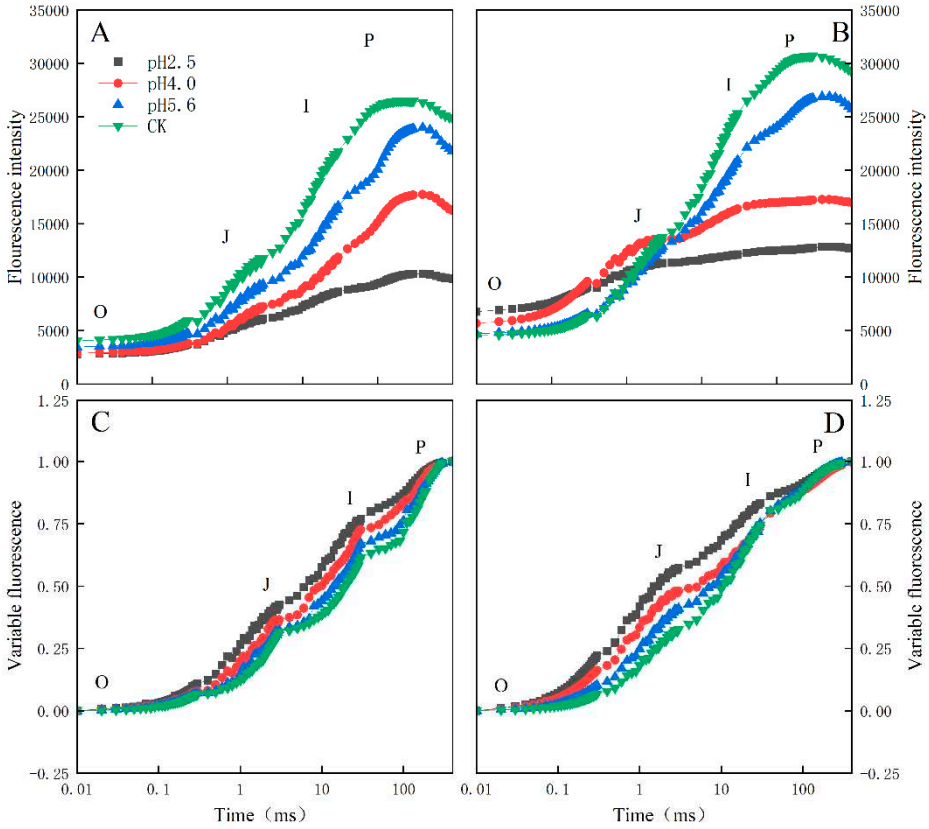

Figure 4. Chlorophyll A fluorescence kinetics curve and chlorophyll a fluorescence standardized curve of PM (A, C) and CL (B, D) under SAR stress conditions. Each curve represents the average data of five replicates.

The normalized OJIP curves for both PM and CL indicated that the O–P points increased as the pH of the SAR solution decreased (relative to the control O–P points) (Figure 4). There were also increasing trends in V_J and V_I for both PM and CL (Figure 5). For PM, V_J and V_I did not change significantly at pH 5.6, but they increased significantly at pH 4.0. For CL, V_J increased significantly at pH 5.6.

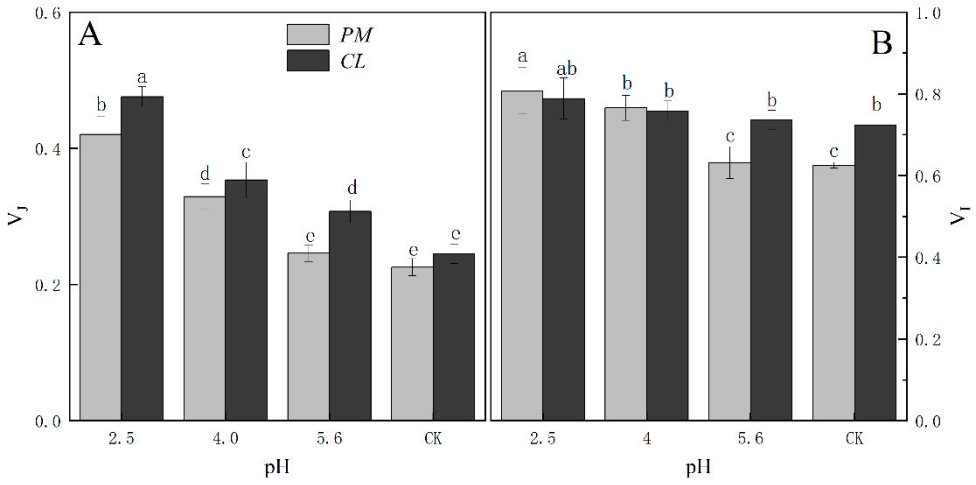

Figure 5. A) Changes in the J point variable fluorescence of PM and CL under SAR stress conditions. (B) Changes in the I point variable fluorescence of PM and CL under SAR stress conditions. $V_I = (F_I - F_O)/(F_M - F_O)$ and $V_J = (F_J - F_O)/(F_M - F_O)$.

Preprints (www.preprints.org) | NOT PEER-REVIEWED | Posted: 10 January 2024 doi:10.20944/preprints202401.0791.v1

The fluorescence increase kinetics of PM and CL were normalized between the O point (50 μs) and the K point (300 μs) as follows: $V_{OK} = (F_T - F_O)/(F_K - F_O)$. The K-band of both species was already higher than that of the control at pH 5.6. Further decreases in the pH resulted in significant increases in the K-band (Figure 6).

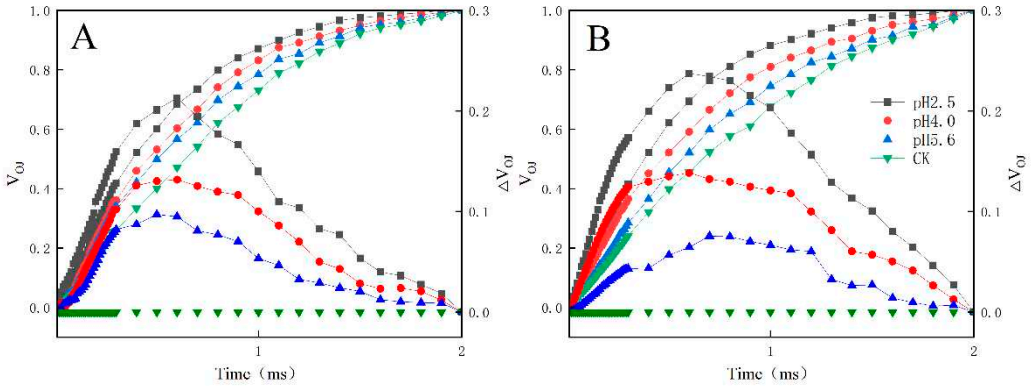

Figure 6. Changes in the K-bands of PM (A) and CL (B) in response to SAR stress. $V_{OJ} = (F_T - F_O)/(F_J - F_O)$ and $\Delta V_{OJ} = V_{OJ}$(treatment) − V_{OJ}(control).

For both PM and CL, the L-band was detected at pH 5.6. Further decreases in the pH were accompanied by significant increases in the L-band. Notably, the L-band of CL was higher than that of PM at pH 2.5 (Figure 7).

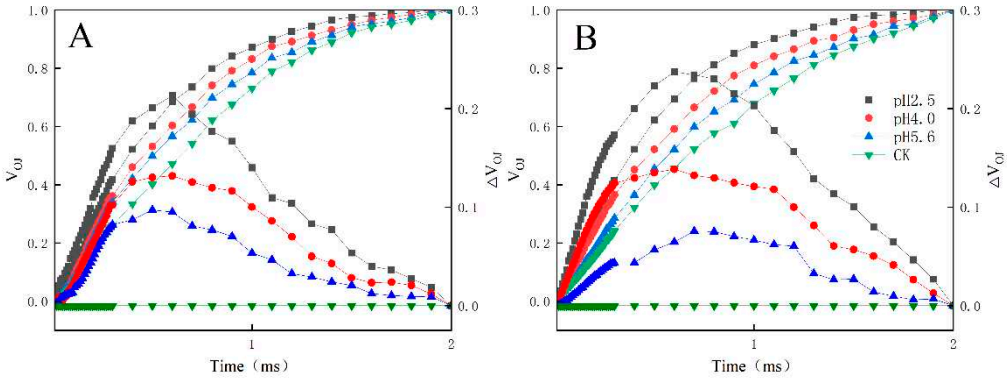

Figure 7. Changes in the L-bands of PM (A) and CL (B) in response to SAR stress. $V_{OK} = (F_K - F_O)/(F_M - F_O)$ and $\Delta V_{OK} = V_{OK}$(treatment) − V_{OK}(control).

For both PM and CL, the SAR treatments altered the amplitude and shape of the DF induction curves (Figure 8A,B). The DF curve decreased as the pH of the SAR solution decreased , with the I_1 peak decreasing faster than the I_2 peak. As the pH value decreased, the I_2:I_1 ratio increased significantly, especially at pH 2.5 and 4.0. The I_2:I_1 ratio increased significantly at pH 5.6, but only for CL.

Preprints (www.preprints.org) | NOT PEER-REVIEWED | Posted: 10 January 2024 doi:10.20944/preprints202401.0791.v1

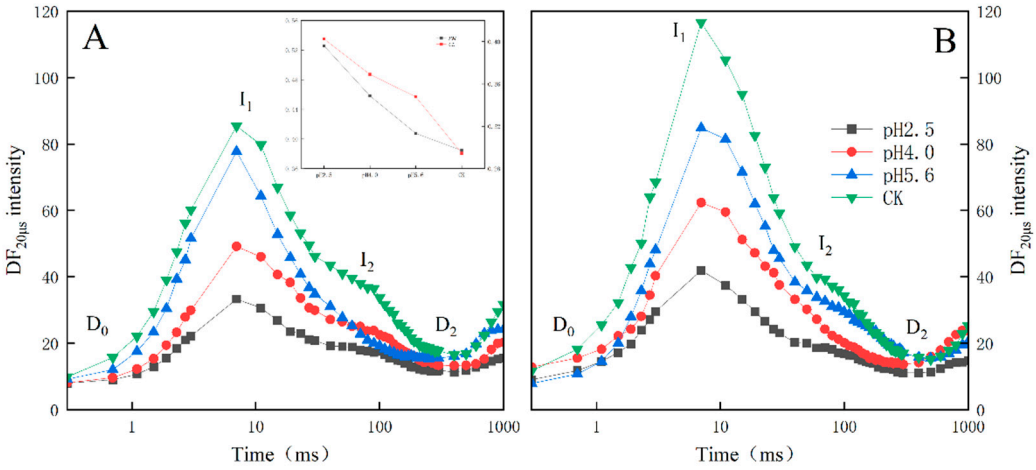

Figure 8. Delayed fluorescence induction curves of PM (A) and CL (B) under SAR stress conditions. Each curve represents the average data of five replicates.

The exposure to various levels of SAR stress led to significant changes to the MR/MR$_0$ kinetics curves for both PM and CL, although the changes were greater for CL (Figure 9). Decreases in the pH of the SAR solution shifted the lowest point of the MR/MR$_0$ kinetics curve to a later time-point. At pH 2.5, both the descending and ascending slopes were lower for CL than for PM (Figure 10).

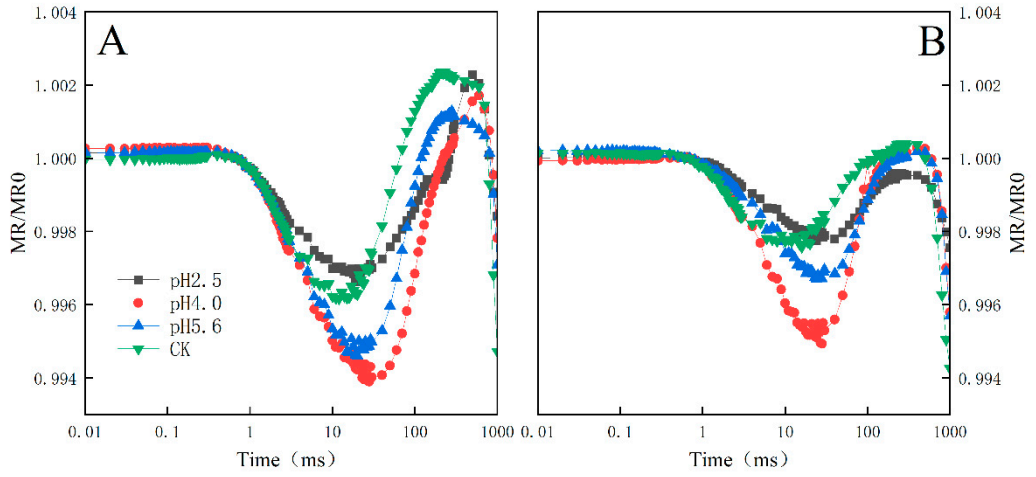

Figure 9. MR$_{820}$ curves of PM (A) and CL (B) under SAR stress conditions. Each curve represents the average data of five replicates.

Preprints (www.preprints.org) | NOT PEER-REVIEWED | Posted: 10 January 2024 doi:10.20944/preprints202401.0791.v1

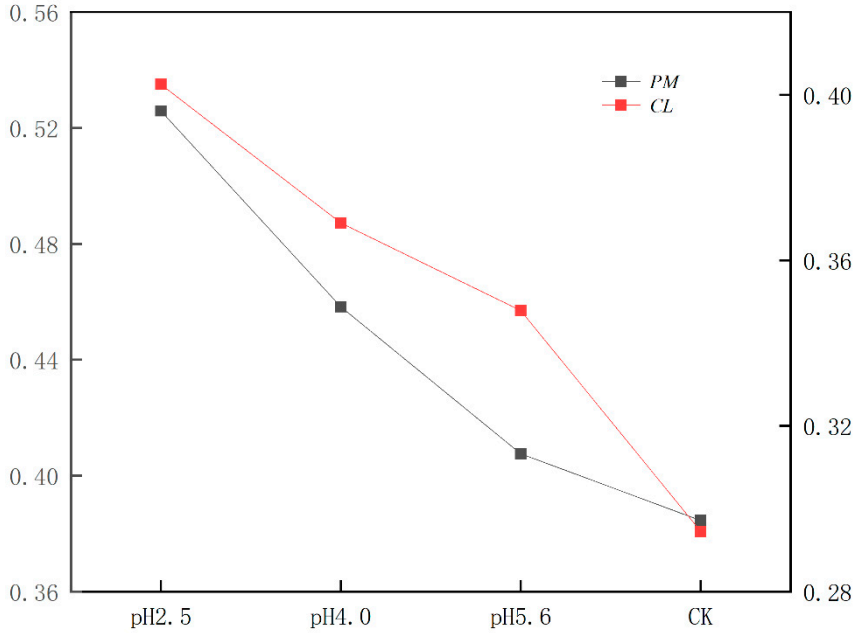

Figure 10. Gradient of the MR_{820} curves of PM and CL under SAR stress conditions. Each curve represents the average data of five replicates.

The SAR treatments decreased ABS/CS_m, TR_O/CS_m, ET_O/CS_m, φP_O, φE_O, ψ_O, PI_{ABS}, and PI_{TOTAL} in both PM and CL, whereas they increased DI_O/CS_m and φD_O. However, there were differences between the two species. Specifically, decreases in pH resulted in increases and decreases in δR_O for PM and CL, respectively. Furthermore, significant decreases in various parameters, including ABS/CS_m, TR_O/CS_m, φP_O, and φE_O, were detected at pH 4.0 and 5.6 for PM and CL, respectively.

3. Discussion

The harmful effects of SAR on plants are reflected by damaged leaf structures and decreased chlorophyll contents, which have inhibitory effects on photosynthesis (Du et al., 2017). Additionally, SAR-induced damages to the stomata and cell membranes of leaves adversely affect plant respiration and other physiological activities (Sant'Anna-Santos et al., 2006). The chlorophyll content, Pn, and Gs decreased significantly in the PM and CL leaves after the SAR pH 4.0 and 2.5 treatments, whereas Ci increased as the pH decreased, implying the decrease in photosynthetic performance in PM and CL was unrelated to stomatal factors.

The main phases of the OJIP curve in response to SAR stress differed between the two analyzed tree species. Specifically, the I–P phase decreased more significantly for CL than for PM. The comparison with CL indicated the fluorescence peak (F_O) increased more in PM as the pH decreased and the I–P phase decreased more under low-pH conditions, eventually resulting in the loss of the P point (Figure 4). The increase in chlorophyll a fluorescence during the J–I phase reflects the extent of the conversion from QA^- to QA, whereas the decrease in the PQ pool leads to a decrease in the primary electron acceptor QA levels because of the limited induction of PQ reduction (Bhatt et al., 2023). The I point represents the equilibrium between the reduction of the PQ pool by the electrons of PSII and the re-oxidation of the PQ pool, whereas the P point represents the completion of the reduction of all electron acceptors in PSII and PSI (Yang et al., 2023). In the current study, the I–P phase, which is related to the PSI activity, indicated that the low-pH SAR treatment inhibited the electron transfer process in PM and CL. More specifically, blocking the transfer of electrons on the PSII receptor side will lead to an increase in the cyclic electron flow around PSI, thereby affecting the reduction and re-oxidation of the PQ pool. Furthermore, under low-pH SAR stress conditions, the OJIP curve gradually changes to the OKJIP curve, with the K point detected at approximately 300 μs.

 doi:10.20944/preprints202401.0791.v1

The appearance of the K point is mainly due to the inhibition of H_2O splitting and the damage to the OEC caused by the partial inhibition of QA, indicative of further damages to PSII.

An increase in V_J is usually indicative of the accelerated restoration of QA, leading to a substantial accumulation of QA in the PS II RC, which then inhibits the transfer of electrons on the receptor side (Goltsev et al., 2016). A previous study showed V_I reflects the capacity of PS I and its receptor quinone to oxidize and reduce (Strasser et al., 2010). Under stress conditions, changes in V_I reportedly represent decreases in the acceptance of electrons by PQ, leading to the inhibited transfer of electrons from QA to QB (Goltsev et al., 2016). In the present study, the SAR treatments of PM and CL had detrimental effects on the ability to accept electrons from PQ, resulting in the accumulation of QA and the inability to transfer electrons from QA to QB (Figure 5).

A damaged OEC (commonly indicated by V_{OK}) obstructs the transfer of electrons from the primary electron donor to the secondary electron donor and leads to an imbalanced electron flow between the donor and receptor sides (Salim et al., 2021). The ΔV_{OK} value represents the standardized V_{OK} value. The V_{OJ} value indicates that the rate of electrons captured by the pigments in the PS II RC exceeds the rate of the exchange between QA^- at the QB site and the oxidized PQ pool (Salim et al., 2021). The ΔV_{OJ} value represents the standardized V_{OJ} value. In this study, a decrease in the pH of the SAR solution negatively affected both V_{OK} and V_{OJ}. As the pH decreased, ΔV_{OK} and ΔV_{OJ} increased, but there were significant differences between CL and PM at pH 2.5 (Figures 6 and 7).

When electrons are transferred to the PSII RCs, the associated DF is caused by the reverse flow of electrons, leading to a charge recombination and the subsequent re-population of the PSII antenna chlorophylls (Goltsev et al., 2009; Strasser et al., 2010). The intensity of DF directly depends on the rate of the reverse electron transfer reaction in the PSII RCs (Van Gorkom et al., 1973;Jursinic et al., 1986). The shape of the induced DF curve varies among sample types and physiological states (Goltsev et al., 1997;Srivastava et al., 1999; Strasser et al., 2010), but it also depends on DF kinetics (Zaharieva et al., 2003). The induced DF curve was constructed using DF signals recorded at the same decay time-points in multiple DF decay curves (Figure 8). In the DF curve, the peak value at 3 ms was designated as I_1, the peak value at approximately 100 ms was designated as I_2, the initial minimum value was designated as D_0, and the final plateau was designated as D_2. After the SAR treatment, the DF curve decreased as the pH decreased, with faster decreases in the I_1 peak than in the I_2 peak.

Typical 820 nm kinetics curve include a decreasing phase followed by an increasing phase. The decrease reflects the oxidation of PSI and PC, whereas the subsequent increase is indicative of the reduction of PSI and PC. At the lowest point of the decreasing phase, the PC and PSI reduction rates are equal to their oxidation rates (Strasser et al., 2010). The 820 nm optical reflectance curve is commonly used to represent the effects of different treatments on PSI (Oukarroum et al., 2013). The MR/MR_0 value was calculated, where MR_0 is the value at the onset of the actinic illumination (0.7 ms; the first reliable MR measurement). An increase in MR/MR_0 indicates a decrease in the concentration of the oxidized states of plastocyanin (PC^+) and the PSI RC ($P700^+$), which is due to the reduction of PC^+ and $P700^+$ (Strasser et al, 2010). Decreases in the pH of the SAR solution decreased the lowest point of the MR curve and shifted the lowest point to a later time-point (Figure 9). At pH 4.0, the slope of the curves for PM and CL decreased significantly (Figure 10), indicative of the severity of the SAR stress. Notably, the decrease in the slope was greater for CL than for PM, implying PM is more tolerant to SAR stress than CL.

According to earlier research, ABS/CS_m, TR_O/CS_m, ET_O/CS_m, and DI_O/CS_m reflect the efficiency of each index per cross-section unit at $t = t_{FM}$ (Stirbet et al., 2011). In the present study, the exposure to SAR stress significantly decreased ABS/CS_m, TR_O/CS_m, and ET_O/CS_m, but increased DI_O/CS_m (Figure 11). The decrease in ABS/CS_m was due to the deactivation of the RCs caused by SAR as well as the destruction of the antenna pigment structure, which decreased the captured light energy and the excitation energy and reduction energy of the RC, while also altering the transfer of electrons. The increase in DI_O/CS_m suggests the SAR treatments activated a defense mechanism through which excess excitation energy in the leaves was dissipated in a timely manner to limit damages. Additionally, φP_O, φD_O φE_O, and Ψ_O are important quantum indicators for the electron transport chain (Figure 11; Wang et al., 2021). Furthermore, δR_O represents the efficiency with which electrons

Preprints (www.preprints.org) | NOT PEER-REVIEWED | Posted: 10 January 2024 doi:10.20944/preprints202401.0791.v1

are transferred from the reduction system to the PSI electron acceptor side; it is also a photosynthetic performance index that is based on light absorption (PI_{ABS}), making it an important parameter for studying the plant photosynthetic status. In this study as well as in earlier studies, PI_{TOTAL} served as the comprehensive photosynthetic performance index (Figure 11; Zhou et al., 2019). Under SAR stress conditions, φP_O, φE_O, Ψ_O, PI_{ABS}, and PI_{TOTAL} decreased significantly for both PM and CL, which was in contrast to the significant increase in φD_O. For PM, the change in δR_O in response to decreases in pH indicates that PSI was more involved in the cyclic transfer of electrons than in the linear transfer of electrons. Increases in cyclic electron transfer are critical for minimizing the SAR-induced damages to the photosynthetic system. According to the change in δR_O, PSI in PM likely mainly contributed to cyclic electron flow, with the dissipation of excess energy decreasing ROS production.

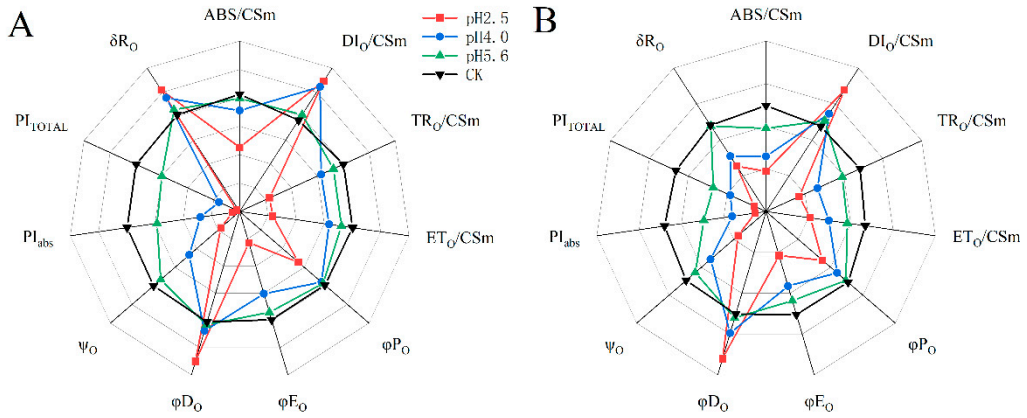

Figure 11. Radar maps of the JIP-test parameters derived from the OJIP transient curves of the chlorophyll A fluorescence of PM (A) and CL (B) under SAR stress conditions. For each parameter, the value for the comparison was set to 1.

4. Materials and Methods

4.1. Plant materials and treatments

Two-year-old PM and CL seedlings that were similar in height were used in this study. The seedlings were obtained from Jiujiang Decheng Landscape Greening Co., Ltd. (Jiangxi, China) and then grown in plastic tubes (60 cm tall, 2 cm upper diameter) filled with a 1:1:3 (v/v) mixture of vermiculite, perlite, and peat soil. Plants were grown outdoors at Jiyang College in Zhuji, Zhejiang, China. Approximately 3 months later, 48 PM and CL seedlings were transferred to two growth chambers. The settings for both growth chambers were as follows: 14-h photoperiod with a photosynthetic photon flux density (PPFD) of approximately 600 mol m^{-2} s^{-1}; relative humidity of approximately 50%; and 25 °C (day)/20 °C night cycle. Fertilizer-containing water along with half-strength Hoagland solution were applied to the plants once per week.

Based on the chemical composition of the acid rain in Zhejiang province in the previous 3 years, H_2SO_4 and HNO_3 (concentration of 98%) were used to prepare the acid rain stock solution (molar ratio of SO_4^{2-} to NO_3^- of 2.4:1 and pH 1.0). The stock solution was diluted with deionized water to prepare SAR solutions with varying pH values (2.5, 4.0, and 5.6) that corresponded to different SAR stress levels. Deionized water (pH 6.8) was used for the control treatment. The leaves of PM and CL seedlings (from top to bottom) were sprayed uniformly with the SAR solutions once every 2 weeks.

4.2. Gas exchange measurements

The LI-6400 portable photosynthesis system (LI-COR, Lincoln, NE, USA) was used to measure the gas exchange parameters of PM and CL. Specifically, The third pair of intact functional leaves from the top of the seedling stem were analyzed, with three replicates per leaf. The measurements

 doi:10.20944/preprints202401.0791.v1

were conducted using the built-in red–blue light source, with a PPFD of 1,200 μmol m^{-2} s^{-1}, a CO_2 concentration of 400 μmol m^{-2} s^{-1}, a leaf chamber temperature of 25 °C, and a flow rate of 300 mmol/s. During the measurements, leaves took over the whole chamber room to ensure smooth progress.

4.3. Determination of the chlorophyll content

The third pair of intact functional leaves from the top of the seedling stem were collected for the determination of the chlorophyll content as described by Lichtenthaler (1983).

4.4. Simultaneous measurement of PF, DF, and MR kinetics

The third pair of intact functional leaves from the top of the seedling stem was selected and maintained in darkness for 30 min. The chlorophyll fluorescence parameters were measured using M-PEA (Hannsatech Instruments Ltd., UK). A red-light pulse (650 nm, 3,500 μmol m^{-2} s^{-1}) resulted in an increase in the fluorescence curve. In terms of the chlorophyll fluorescence curve, O represents the initial fluorescence level; K (300 μs), J (2–3 ms), and I (30 ms) represent the intermediate fluorescence levels; and P (500 ms) represents the peak fluorescence level. We also used the JIP-test to analyze the OJIP fluorescence transients (Strasser et al., 2004; Stirbet and Govindjee, 2011). The JIP-test defines the maximum energy flux of absorption (ABS), trapping (TR), electron transport (ET), and dissipation (DI) in the excitation cross-section (CS) cascade. This test is based on the basic theory of energy flow through the thylakoid membrane and the total energy flow from the collecting complex (i.e., energy flux ratio).

The data were analyzed using the JIP-test (Strasser et al, 2004). Several basic data were collected in this study, including the following: F_O (fluorescence intensity at 20 μs), F_L (fluorescence intensity at 150 μs), F_K (fluorescence intensity at 300 μs), F_J (fluorescence intensity at 2 ms), F_I (fluorescence intensity at 30 ms), and F_M (maximum fluorescence intensity, which is equal to F_P). To analyze the electron transport chain activity, the following relative fluorescence parameters were calculated via the double-normalization of the moment chlorophyll fluorescence values against the end points in different time intervals in the OJIP part of the transient: OP, OK, OJ, OI, and IP; V_T, relative variable fluorescence at time T, which is calculated using the formula $V_T = (F_T - F_O)/(F_M - F_O)$; W_{OK}, ratio of the variable fluorescence ($F_T - F_O$) to the amplitude ($F_K - F_O$), which is used to represent the L-band; and W_{OJ}, which is calculated using the formula $W_{OJ} = (F_T - F_O)/(F_J - F_O)$ and used to represent the K-band.

The parameters that refer to time 0 include the following: the maximum quantum yield of PSII primary photochemistry ($\varphi P_O = TR_O/ABS = F_V/F_M$); the efficiency with which a trapped exciton moves an electron into the electron transport chain beyond the reduced QA form (QA^-) ($\psi E_O = ET_O/TR_O$); the quantum yield of electron transport ($\varphi E_O = ET_O/ABS$); the average fraction of open PSII RCs in the time interval between 0 and t_{FM} (S_m/t_{FM}); the fraction of active PSII RCs per CS (RC/CS); absorption flux per CS (ABS/CS); trapped energy flux per CS (TR_O/CS); electron transport flux per CS (ET_O/CS); absorption flux per RC (ABS/RC); the quantum yield for the reduction of the end electron acceptors on the PSI acceptor side ($\varphi R_O = RE_O/ABS$); and the probability that an electron is transported from the reduced intersystem electron acceptors to the final electron acceptors of PSI [$\delta R_O = RE_O/ET_O = (1 - V_I)/(1 - V_J)$].

4.5. Data analysis

All experiments were repeated at least three times. All values are expressed herein as the mean ± standard deviation. A one-way ANOVA was performed using SPSS (SPSS Inc.). The Duncan test was used to compare mean values, with $P < 0.05$ set as the threshold for determining significance.

5. Conclusions

The SAR treatments in this study damaged the cell membranes and stomata of PM and CL, resulting in decreased chlorophyll contents. The I–P phase decrease was due to the inhibited transfer of electrons on the electron acceptor side of PSI, which resulted in an increase in cyclic electron flow around PSI. The increase in chlorophyll a fluorescence during the J–I phase, which was indicated by

 doi:10.20944/preprints202401.0791.v1

V_J and V_I, reflected the extensive transfer of electrons from PSI to the PQ pool. However, the re-oxidation of the PQ pool was insufficient, leading to the accumulation of QA^-. The appearance of the L-band and K-band demonstrates that SAR stress interferes with the transfer of electrons on the donor and acceptor sides, thereby decreasing the transfer of energy to the active RC of PSII. This results in the dissociation of the PSII antenna complex from the PSII core proteins, which adversely affects the OEC and destabilizes the PSII system. In terms of the JIP-test parameters, ABS/CS_m, TR_O/CS_m, ET_O/CS_m, φP_O, φE_O, and Ψ_O decreased significantly after the SAR treatments, resulting in decreases in PI_{ABS} and PI_{TOTAL}. Furthermore, the SAR-induced increases in both DI_O/CS_m and φD_O protected PSII from membrane photooxidation. Decreases in pH caused δR_O to increase, but only for PM. In conclusion, the decrease in chlorophyll contents and the damages to the OEC in PM and CL disrupted the transfer of electrons on the donor and acceptor sides of PSII, ultimately resulting in increased chlorophyll fluorescence and thermal dissipation, which inhibited photosynthesis (Pn) and suppressed the growth of PM and CL. However, PM was more tolerant to SAR than CL, which may be related to the observed difference in δR_O between the two tree species. Thus, the physiological functions of CL may already be damaged at pH 5.6, while those of PM are generally unaffected until the pH decreases to 4.0.

Author Contributions: Conceptualization, Pengzhou Shu and Xueqin Li; Data curation, Pengzhou Shu and Xueqin Li; Funding acquisition, Songheng Jin; Investigation, Zhongxu Wang and Penghong Qian; Methodology, Yanlei Du and Yini Han; Resources, Pengzhou Shu and Xueqin Li; Software, Xiaofei Gong; Validation, Pengzhou Shu and Xueqin Li; Writing – original draft, Pengzhou Shu and Xueqin Li; Writing – review & editing, Pengzhou Shu and Xueqin Li.

Funding: This research was funded by the National Key Research and Development Project (2019YFE0118900), the National Natural Science Foundation of China (31971641), and Zhejiang Provincial Team Science and Technology Commissioner Project (Horticulture Team in Wencheng).

Conflicts of Interest: The authors declare that the research was conducted in the absence of any commercial or financial relationships that could be construed as a potential conflict of interest.

References

Berger, T. W., Turtscher, S., Berger, P., & Lindebner, L. (2016). A slight recovery of soils from Acid Rain over the last three decades is not reflected in the macro nutrition of beech (Fagus sylvatica) at 97 forest stands of the Vienna Woods. Environment Pollution, 216, 624-635.

Bhatt U., Sharma S.,Kalaji H.M., Strasser R.J.,Chomontowski C.,Soni V. (2023) Sunlight-induced repair of photosystem II in moss Semibarbula orientalis under submergence stress. Functional Plant Biology 50, 777-791.

Chen S , Yang J , Zhang M ,et al.(2015) .Classification and characteristics of heat tolerance in Ageratina adenophora populations using fast chlorophyll a fluorescence rise O-J-I-P.Environmental and Experimental Botany, 122:126-140.

Chen, S., Zhang, X., Liu, Y., Hu, Z., Shen, X., & Ren, J. (2015). Simulated acid rain changed the proportion of heterotrophic respiration in soil respiration in a subtropical secondary forest. Applied Soil Ecology, 86, 148-157.

Chen, S., Zhang, X., Sang, L., Sun, L., & Wu, J. (2021). Simulated acid rain offset a warming-induced increase in soil respiration but did not impact the temperature sensitivity of soil respiration in a cropland. Applied Soil Ecology, 164.

Diatta, J., Youssef, N., Tylman, O., Grzebisz, W., Markert, B., Drobek, L., Lejwoda, P. (2021). Acid rain induced leakage of Ca, Mg, Zn, Fe from plant photosynthetic organs – Testing for deciduous and dicotyledons. Ecological Indicators, 121.

Dou R.Q., Xie Y.L., Liu Frank X., Wang B., Xu F., Xiao K.M.(2023) In situ mycoremediation of acid rain and heavy metals co-contaminated soil through microbial inoculation with Pleurotus ostreatus, Science of The Total Environment,169020.

Du E.Z., Dong D., Zeng X.T., Sun Z.Z., Jiang X.F., Vries W.D.(2017), Direct effect of acid rain on leaf chlorophyll content of terrestrial plants in China, Science of The Total Environment.

Du, E., Dong, D., Zeng, X., Sun, Z., Jiang, X., & de Vries, W. (2017). Direct effect of acid rain on leaf chlorophyll content of terrestrial plants in China. Sci Total Environ, 605-606, 764-769.

Goltsev V, Yordanov I (1997) Mathematical model of prompt and delayed chlorophyll fluorescence induction kinetics. Photosynthetica 33: 571–586.

Goltsev, V. N., Kalaji, H. M., Paunov, M., Bąba, W., Horaczek, T., Mojski, J.,Allakhverdiev, S. I. (2016). Variable chlorophyll fluorescence and its use for assessing physiological condition of plant photosynthetic apparatus. Russian Journal of Plant Physiology, 63(6), 869-893.

Guo, Y., Zhang, Y., Lu, Y., Shi, J., Chen, S., Strasser, R. J., . . . Hu, Z. (2020). Special issue in honour of Prof. Reto J. Strasser - Effect of AtLFNR1 deficiency on chlorophyll a fluorescence rise kinetics OJIP of Arabidopsis. Photosynthetica, 58(SPECIAL ISSUE), 391-398.

Jiang C.W., Xu Q., Zhang B.B, Gao D.Q., Ma Y.B.(2017). Research Progress on Photosynthetic Physiology and Resource Utilization Efficiency of Pinus massoniana Pinus massoniana Lamb [J]. World Forestry Research, 30(04): 24-28.

Jursinic P (1986) Delayed fluorescence: current concepts and status. In: Govindjee, Amesz J, Fork DJ, editors. Light emission by plants and bacteria.Academic Press, Orlando. 291–328.

Li Q.Y., Liu X., Zhang J.C.(2021). Research on the Trend of Acid Rain Transformation in the Yangtze River Delta Region [J]. Journal of Nanjing Forestry University (Natural Sciences Edition), 45(01): 168-174.

Li, Y., Wang, Y., & Zhang, W. (2021). Impact of simulated acid rain on the composition of soil microbial communities and soil respiration in typical subtropical forests in Southwest China. Ecotoxicol Environ Saf, 215, 112152.

Liang J, Mai B.R, Zheng Y.F, et al. (2008).Effects of simulated acid rain on the growth, yield, and quality of Brassica napus L. [J]. Journal of Ecology(01): 274-283

Ling D.J., Huang Q.C., Ouyang Y. (2010), Impacts of simulated acid rain on soil enzyme activities in a latosol, Ecotoxicology and Environmental Safety,

Liu Y.Y., Jiang H, Li Y.H., Yuan H.Y.(2010). Short-term Effects of Simulated Acid Rain on Soil Respiration in Cunninghamia lanceolata (Lamb.) Hook. Seedling-Soil System. Acta Ecologica Sinica, 30(08): 2010-2017.

Liu, J.Guo, Y. Y.Bai, Y. W.Camberato, J. J.Xue, J. Q.Zhang, R.H.(2018).Effects of Drought Stress on the Photosynthesis in Maize.Russian Journal of Plant Physiology, 65(6).

Liu, Z., Wei, H., Zhang, J., Wang, T., He, Y., Zhong, J., & Ma, R. (2021). Increasing acid rain frequency promotes the microbial community dissimilarities of forest soil rather than agricultural soil in southern China. Ecotoxicol Environ Saf, 230, 113123.

Malla, R., Neupane, P. R., & Köhl, M. (2023). Climate change impacts: Vegetation shift of broad-leaved and coniferous forests. Trees, Forests and People, 14.

Oukarroum A., Gharous M. E., Goltsev V., Strasser R.J.,(2016)Delayed fluorescence emission as a probe for the response of photosynthetic organisms to high temperature exposure: A comparative study,Journal of Luminescence. 180, 321-327.

Oukarroum, A., & Strasser, R. J. (2004). Phenotyping of dark and light adapted barley plants by the fast chlorophyll a fluorescence rise OJIP. South African Journal of Botany, 70(2), 277-283.

Oukarroum, A., Goltsev, V., & Strasser, R. J. (2013). Temperature effects on pea plants probed by simultaneous measurements of the kinetics of prompt fluorescence, delayed fluorescence and modulated 820 nm reflection. PLoS One, 8(3), e59433.

Poschenrieder C, Benet Gunsu, Corrales I, et al. (2008).A glance into aluminum toxicity and resistance[J].Science of The Total Environment, 400(1-3):356-368.

Ren K.X., Chen J.J, Cui T.T., Li M., Zhou C.l., Zhang R.H. , et al. (2017).Effects of salinity on photosynthesis in maize probed by prompt fluorescence, delayed fluorescence and P700 signals[J].Trends in Cell Biology, 27(3).

Salim Akhter, M., Noreen, S., Mahmood, S., Athar, H.-u.-R., Ashraf, M., Abdullah Alsahli, A., & Ahmad, P. (2021). Influence of salinity stress on PSII in barley (Hordeum vulgare L.) genotypes, probed by chlorophyll-a fluorescence. Journal of King Saud University - Science, 33(1).

Sant'Anna-Santos F., B., Campos da Silva, L., Alves Azevedo, A., Marcos de Araújo, J., Figueiredo Alves, E., Antônio Monteiro da Silva, E., & Aguiar, R. (2006). Effects of simulated acid rain on the foliar micromorphology and anatomy of tree tropical species. Environmental and Experimental Botany, 58(1-3), 158-168.

Shen, J., Li, X., Zhu, X., Ding, Z., Huang, X., Chen, X., Jin, S. (2022) Molecular and photosynthetic performance in the yellow leaf mutant of Torreya grandis according to transcriptome sequencing, chlorophyll a fluorescence, and modulated 820 nm reflection. Cells, 11, 431.

Shi, Z., Zhang, J., Xiao, Z., Lu, T., Ren, X., & Wei, H. (2021). Effects of acid rain on plant growth: A meta-analysis. Journal of Environmental Management, 297.

Srivastava A, Strasser RJ, Govindjee (1999) Greening of peas: parallel measurements of 77 K emission spectra, OJIP chlorophyll a fluorescence transient, period four oscillation of the initial fluorescence level, delayed light emission, and P700. Photosynthetica 37: 365–392.

Stirbet, A., & Govindjee. (2011). On the relation between the Kautsky effect (chlorophyll a fluorescence induction) and Photosystem II: Basics and applications of the OJIP fluorescence transient. Journal of Photochemistry and Photobiology B: Biology, 104(1-2), 236-257.

Strasser R J (2004).Analysis of the Chlorophyll a Fluorescence Transient[J].Chlorophyll A Fluorescence A Signature of Photosynthesis.

Strasser RJ, Tsimilli-Michael M, Qiang S, Goltsev V (2010) Simultaneous in vivo recording of prompt and delayed fluorescence and 820-nm reflection changes during drying and after rehydration of the resurrection plant Haberlea rhodopensis. Biochim Biophys Acta 1797: 1313–1326.

Tomlinson, G.H. (2003) Acidic deposition, nutrient leaching and forest growth. Biogeochemistry 65, 51–81

Van Gorkom HJ, Donze M (1973) Charge accumulation in the reaction center of PSII. Photochem Photobiol 17: 333–342.

Yang Q., Guo Y.J., Li J.J., Wang L., Wang H., Liu G.D., Fang W.P., Qiang S., Strasse R. J ., Chen S.G.,(2023) Natural plant inducer 2-Amino-3-Methylhexanoic acid protects physiological activity against high-temperature damage to tea (Camellia sinensis),Scientia Horticulturae. 312,111836.

 doi:10.20944/preprints202401.0791.v1

Zaharieva I, Goltsev V (2003) Advances on PS II investigation by measurement of delayed chlorophyll fluorescence by a phosporoscopic method.Photochem Photobiol 77 292–298.

Zhang, Y., Liang, C. (2023) .Improving yield and quality of rice under acid rain stress by regulating nitrogen assimilation with exogenous Ca2+. Environ Sci Pollut Res 30, 12085–12097.

Zheng, Y., Wang, Y., Zheng, Y., & Li, Y. (2022). Effects of Simulated Acid Rain on Soil Enzyme Activity and Related Chemical Indexes in Woodlands. Forests, 13(6).

Zhou R.H., Kan X., Chen J.J., Hua H.L., Li Y., Ren J.J., et al.(2019).Drought-induced changes in photosynthetic electron transport in maize probed by prompt fluorescence, delayed fluorescence, P700 and cyclic electron flow signals. Environmental and Experimental Botany; 158 , 51-62.

Zushi, K., & Matsuzoe, N. (2017). Using of chlorophyll a fluorescence OJIP transients for sensing salt stress in the leaves and fruits of tomato. Scientia Horticulturae, 219, 216-221.